Local Structure of Intercomponent Energy Transfer in Homogeneous Turbulent Shear Flow

By JAMES G. BRASSEUR† AND MOON J. LEE‡

Intercomponent energy transfer by pressure–strain-rate was investigated for homogeneous turbulent shear flow. The rapid and slow parts of turbulent pressure (decomposed according to the influence of the mean deformation rate) are found to be uncorrelated; this finding provides strong justification for current modeling procedure in which the pressure–strain-rate term is split into the corresponding parts. Issues pertinent to scales involved in the intercomponent energy transfer are addressed in comparison with those for the Reynolds-stress and vorticity fields. A physical picture of the energy transfer process is described from a detailed study of instantaneous events of high transfer regions. It was found that the most significant intercomponent energy transfer events are highly localized in space and are imbedded within a region of concentrated vorticity.

1. Introduction

Statistical quantities in turbulent flows have underlying them local, random events whose dynamical evolution determines the structure of the average. Here, *event* refers to a local concentration of a statistical quantity in an instantaneous turbulent field and *significant events* are those which provide major contributions to the average.

The pressure–strain-rate term is the most controversial in current modeling procedure for the Reynolds-stress transport. The poor understanding of the role played by pressure in intercomponent energy transfer is in part for want of reliable data from laboratory measurements of fluctuating pressure. With the advent of supercomputer, 'data' from full turbulence simulations of building-block flows such as homogeneous turbulence are now available. In this paper, we analyse significant events associated with the intercomponent energy transfer by interaction between fluctuating pressure and strain rate in homogeneous turbulent shear flow.

Homogeneous turbulence is chosen for the present study due to the unambiguous statistical description of intercomponent energy transfer as the correlation between the fluctuating pressure and strain rate. In this study, we consider those local events which do not average to zero. Velocity times pressure-gradient, which appears in the instantaneous Reynolds stress equation, may be written as the sum of transport and trace-free terms. In homogeneous turbulence, the trace-free term (pressure–strain-rate) alone survives on the spatial average due to the requirement of the

translational invariance. In inhomogeneous turbulence, the split of the velocity–pressure-gradient is not unique (Lumley 1975). We hope to extend the inquiry in the future to homogeneous turbulence subjected to irrotational mean strains and to inhomogeneous wall-bounded turbulence.

2. Preliminaries

The transport equation for the Reynolds-stress tensor $\overline{u_i u_j}$ in homogeneous turbulence is given by (Lee & Reynolds 1987)

$$\frac{dR_{ij}}{dt} = P_{ij} + O_{ij} + T_{ij} - D_{ij} \tag{1}$$

where $P_{ij} = -(S_{ik}R_{jk} + S_{jk}R_{ik})$ is the production-rate tensor, $O_{ij} = -(\Omega_{ik}R_{jk} + \Omega_{jk}R_{ik})$ the kinematic rotation term, $T_{ij} = \frac{2}{\rho}\overline{ps_{ij}}$ the pressure–strain-rate term and $D_{ij} = 2\nu\,\overline{u_{i,k}u_{j,k}}$ the 'dissipation-rate' tensor (**u** and p are the fluctuating vector velocity and pressure, respectively; an overbar denotes a statistical average, repeated indices imply summation and a comma followed by an index means differentation). Here, $S_{ij} = \frac{1}{2}(U_{i,j} + U_{j,i})$ and $\Omega_{ij} = \frac{1}{2}(U_{i,j} - U_{j,i})$ are the mean strain-rate and rotation-rate tensors, respectively, and s_{ij} is the turbulent strain-rate tensor. Notice that the kinematic rotation and pressure–strain-rate terms are trace-free ($O_{ii} = 0$ and $T_{ii} = 0$), and hence they do not contribute to production of the turbulent kinetic energy. These terms represent intercomponent transfer of turbulent kinetic energy by the mean rotation rate and by interaction between fluctuating pressure and strain rate, respectively.

For homogeneous shear flow with mean velocity $\mathbf{U} = (Sy, 0, 0)$, equations for the component energy can be written as

$$\left.\begin{aligned}
\frac{d}{dt}\overline{u^2} &= -S\,\overline{uv} &&- S\,\overline{uv} &&+ T_{11} - D_{11},\\
\frac{d}{dt}\overline{v^2} &= -S\,\overline{uv} &&+ S\,\overline{uv} &&+ T_{22} - D_{22},\\
\frac{d}{dt}\overline{w^2} &= &&&&+ T_{33} - D_{33},\\
\frac{d}{dt}\overline{uv} &= -\frac{S}{2}\left(\overline{u^2} + \overline{v^2}\right) &&+ \frac{S}{2}\left(\overline{u^2} - \overline{v^2}\right) &&+ T_{12} - D_{12},
\end{aligned}\right\} \tag{2}$$

where $S = dU/dy$ is the imposed 'shear rate' uniform in space and constant in time.[†] Turbulent shear flow with unidirectional mean velocity has the characteristic that, on the average, turbulent kinetic energy is produced by the mean strain rate in the streamwise component u as much as in the gradient-direction component v (i.e. $P_{11} = P_{22} = -S\overline{uv}$), and the kinematic rotation term rotates the turbulence structure in the xy-plane by transferring energy $-S\,\overline{uv}$ from v-component to u-component. The principal axes of the production-rate tensor are aligned at 45°

---

† For notational convenience, we occasionally shift from (x_1, x_2, x_3) and (u_1, u_2, u_3) to (x, y, z) and (u, v, w).

with those of the mean strain-rate tensor, stretching the principal ellipsoid of the Reynolds-stress tensor, while the kinematic rotation term is perpendicular to the Reynolds-stress tensor, only tilting the principal ellipsoid.

It is suggested by experimental measurements (Harris, Graham & Corrsin 1977; Tavoularis & Corrsin 1981) and numerical simulations (Rogallo 1981; Rogers, Moin & Reynolds 1986; Lee, Kim & Moin 1987) that homogeneous turbulent shear flow approaches an asymptotic growth state in which most turbulent kinetic energy is concentrated in the u-component, followed by w, then v. The u-component loses energy to those in the spanwise (w) and gradient directions (v) through the pressure–strain-rate correlations: $T_{11} < 0$, $T_{22} > 0$ and $T_{33} > 0$. Examination of the process by which the pressure–strain-rate redistributes energy between components and the mechanism by which the spanwise component receives the greater share is the primary purpose of this study.

The equations for fluctuating momentum flux $(u_i u_j)$, which lead to (2) on the average, contain local products of fluctuating pressure and strain rate which by continuity sum to zero at a point $(ps_{ii} = 0)$. The pressure–strain-rate term may therefore be associated with local as well as average intercomponent transfer of kinetic energy. The role of fluctuating pressure as causing the local transfer of kinetic energy between components can be observed more clearly in the instantaneous Fourier-transformed equations; pressure alters the directional distribution of the energy associated with individual Fourier modes without modifying their energy content (Batchelor 1953, §5.2).

The present investigation makes use of the full simulation of homogeneous turbulent shear flow (Rogers *et al.* 1986). The simulation was carried out by using a pseudospectral code developed by Rogallo (1981) with periodic boundary conditions on a grid with $128 \times 128 \times 128$ node points. Run R128 (vid. Rogers *et al.*) was analysed for fields at $\beta = 4$ and 8 ($\beta = St$ is the total shear). The run was made by imposing a homogeneous shear rate on an initially isotropic turbulence with an energy spectrum $E(k)$ of a top-hat profile. As the flow developed, reasonable values of velocity-derivative skewness were attained and the largest scales approached the size of the computational domain near $\beta = 16$. The Taylor-microscale Reynolds number ranged from 43 to 74 for $\beta = 4$–8, and the ratio of turbulence time scale to that of the mean field (Sq^2/ϵ where $q^2 = R_{ii}$ and $\epsilon = \frac{1}{2}D_{ii}$) increased from 5.4 to 8.8 between $\beta = 4$ and 8.

3. Characteristics of rapid and slow pressures

The Poisson equation for fluctuating pressure in homogeneous shear flow

$$-\frac{1}{\rho}\nabla^2 p = 2S\,u_{2,1} + u_{i,j}u_{j,i} \tag{3}$$

can be decomposed into two parts, *rapid* and *slow* pressures:

$$-\frac{1}{\rho}\nabla^2 p_{\mathrm{r}} = 2S\,u_{2,1} \qquad \text{and} \qquad -\frac{1}{\rho}\nabla^2 p_{\mathrm{s}} = u_{i,j}u_{j,i}. \tag{4}$$
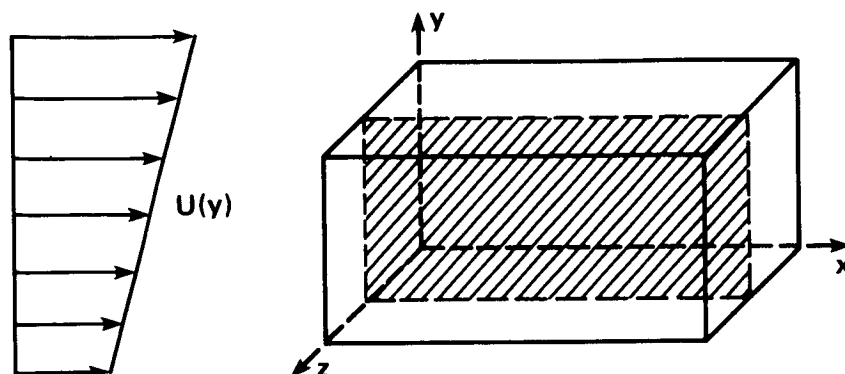
FIGURE 1. The hatched area in the one-eighth (1/8) of the whole computational domain indicates the xy-plane over which the two-dimensional contours in figures 2, 3 and 5 are displayed. The streamwise extent of this 64 × 64 × 64 subdomain is twice those in the spanwise and gradient directions.

From this decomposition it is apparent that the rapid pressure responds directly to the mean velocity gradient, whereas the slow pressure is affected only indirectly by the mean, via the fluctuating velocity gradients.

In accord with this, the pressure–strain-rate term may be separated into *rapid* and *slow* parts:

$$T_{ij} = \Pi_{ij} + \Phi_{ij} \tag{5}$$

where

$$\Pi_{ij} = \frac{2}{\rho}\,\overline{p_r s_{ij}} \quad \text{and} \quad \Phi_{ij} = \frac{2}{\rho}\,\overline{p_s s_{ij}}. \tag{6}$$

In Reynolds-stress transport closures (e.g. Launder, Reece & Rodi 1975; Lumley 1978) these terms have been modeled separately, the slow pressure–strain-rate term typically with a 'return-to-isotropy' model. Order-of-magnitude arguments would suggest that the slow pressure resides in scales of the same order as the energy-containing eddies and the rapid pressure in somewhat larger scales, albeit it is not obvious in what scales the pressure–strain-rate events are likely to reside.

At an earlier time ($\beta = 4$), the rapid pressure variance $\overline{p_r^2}$ is 70% of the complete pressure variance $\overline{p^2}$ and reaches 87% at a later time ($\beta = 8$), indicating increasingly dominant contribution of the rapid part to the complete pressure fluctuations.[†] These figures compare with values in turbulent channel flow (e.g. Kim, Moin & Moser 1987) of 50% in the sublayer to 30% outside (P. Bradshaw 1987, private communication). In the homogeneous shear flow, r.m.s. rapid pressure p_r' dominates r.m.s. slow pressure p_s' by a factor of two at both times.

[†] It has been suggested (P. Bradshaw 1987, private communication) that the term 'complete pressure' be adopted to describe the sum of rapid and slow pressures to avoid confusion with either the full pressure (mean plus fluctuating parts) or the total pressure (static plus dynamic pressures).
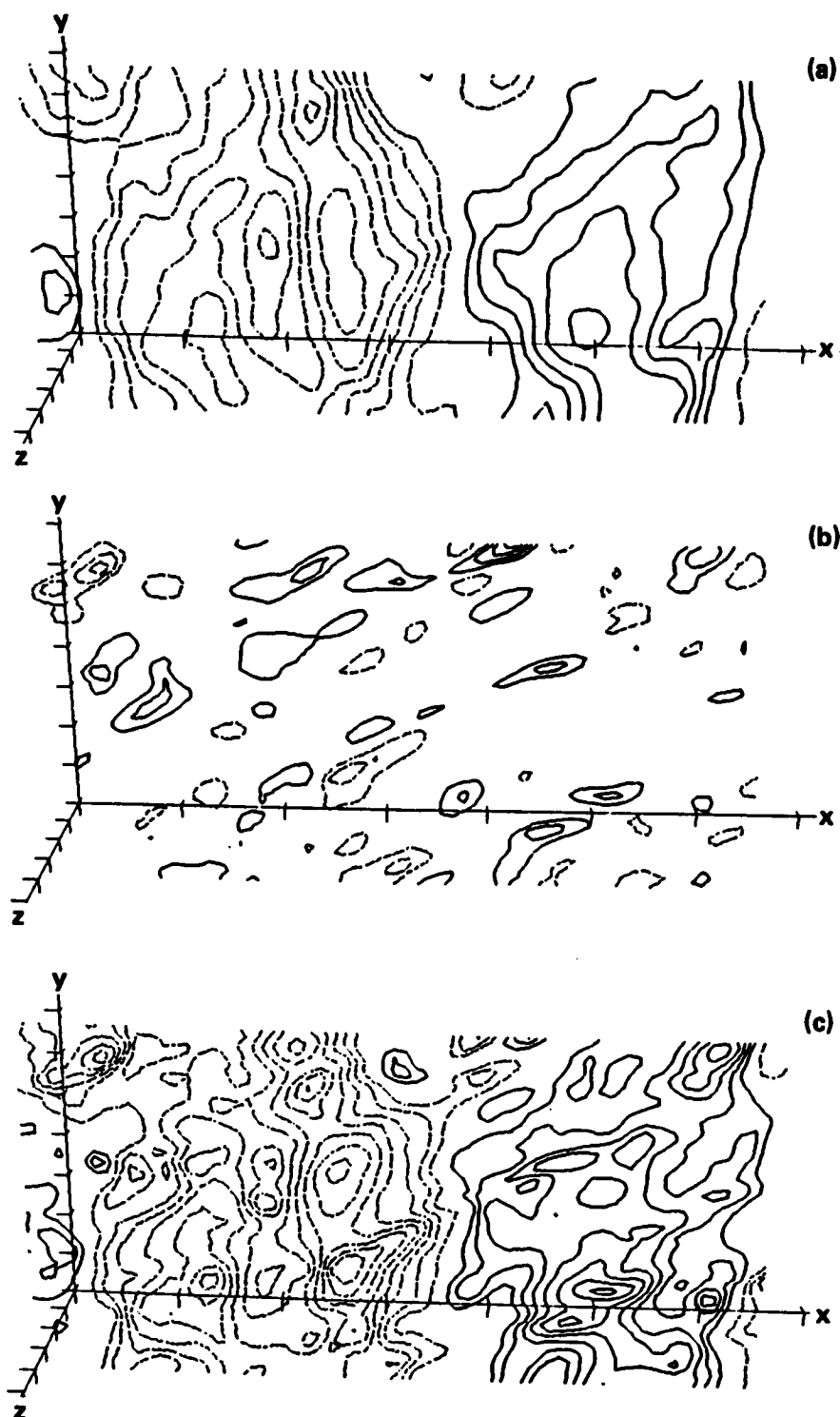
FIGURE 2. Contours of constant pressure on the xy-plane in figure 1 ($\beta = 8$): (a) rapid pressure, p_r; (b) slow pressure, p_s; (c) complete pressure, $p = p_r + p_s$. ———, negative; ----, positive.
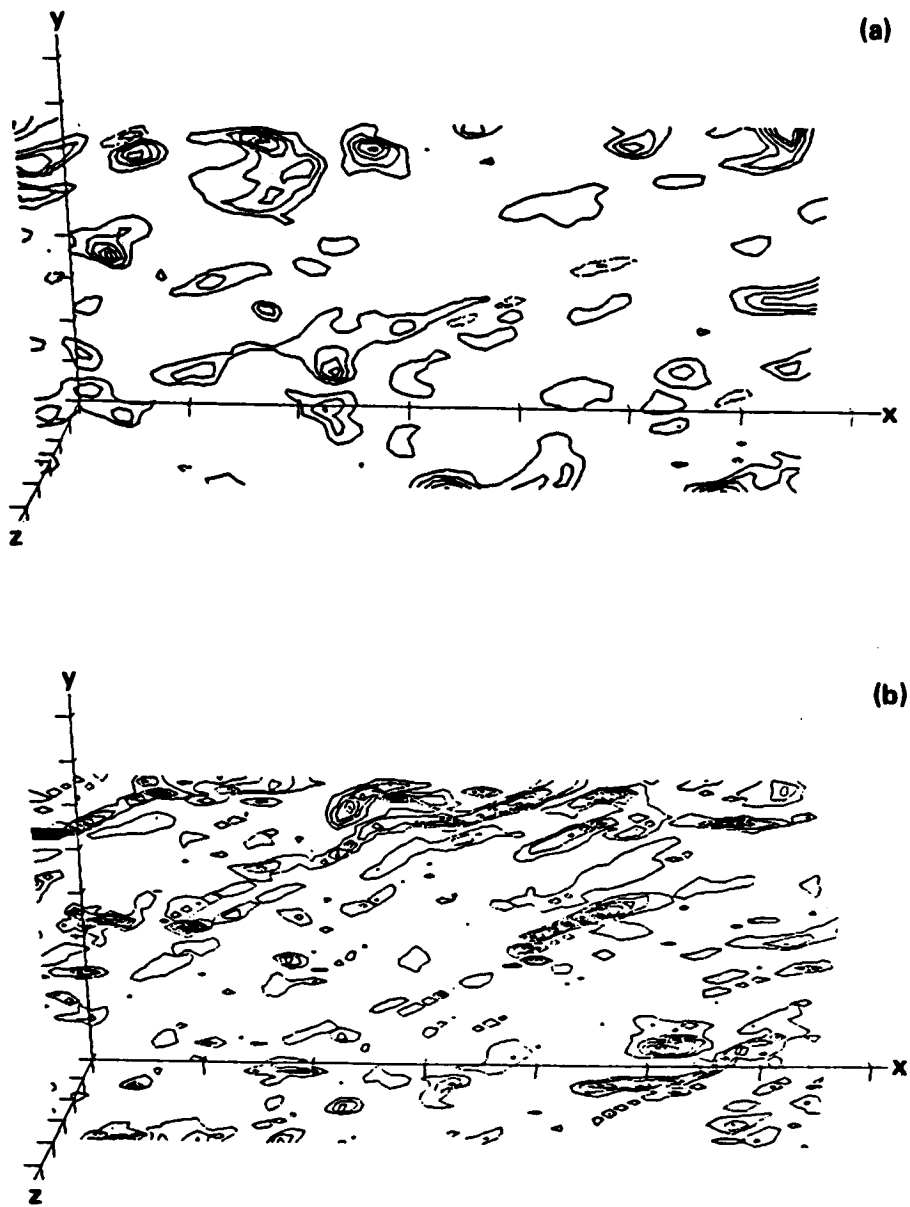
FIGURE 3. Contours on the xy-plane in figure 1 ($\beta = 8$): (a) fluctuating Reynolds stress uv (——, negative; ----, positive); (b) fluctuating vorticity magnitude, $|\omega|^2$.

It was found that the correlation coefficient between the rapid and slow pressures is very small (0.05 at $\beta = 4$ and 0.002 at $\beta = 8$). Note that this fact provides strong support for the modeling procedures in which the pressure–strain-rate term is divided into the rapid and slow parts (Launder *et al.* 1975; Lumley 1978). Since the correlation coefficient between the rapid and slow pressures is almost zero, one would inquire whether they are concentrated in different regions in space.

β	Π_{11}	Φ_{11}	T_{11}	Π_{22}	Φ_{22}	T_{22}	Π_{33}	Φ_{33}	T_{33}
4	−35.9	−16.8	−52.6	−5.2	17.6	12.4	41.1	−0.8	40.3
8	−29.7	−26.1	−55.8	−4.1	24.3	20.2	33.8	1.7	35.5

$$\beta = St; \quad T_{ij} = \Pi_{ij} + \Phi_{ij} \text{ where } \Pi_{ij} = \tfrac{2}{\rho}\,\overline{p_r s_{ij}} \text{ and } \Phi_{ij} = \tfrac{2}{\rho}\,\overline{p_s s_{ij}}.$$

TABLE 1. Components of pressure–strain-rate in homogeneous shear flow.

To address this question, instantaneous pressure fields were studied in detail. Figure 1 shows a schematic of an xy-plane (consisting of 64×64 data points) midway in the spanwise z-direction in a $64 \times 64 \times 64$ subdomain where primary attention is to be paid for the following discussion.† Figures 2(a–c) show contours of constant rapid, slow and complete pressures at $\beta = 8$. It is discernible that variation of rapid pressure is much larger than that of slow pressure. Even more obvious is the substantial difference in scale. Figure 2(a) (and three-dimensional contour plots not shown here) illustrates that rapid pressure is roughly constant in planes perpendicular to the x-axis and the streamwise variation is sinusoidal with about two wavelengths occupying the whole computational domain. On the other hand, figure 2(b) shows spotty distribution of slow pressure. Therefore, the product of this very-large-scale structure of rapid pressure and the much-smaller-scale slow pressure results in a relatively-small-scale structure with average near zero: $\overline{p_r p_s}/(p_r' p_s') \simeq 0$.

Figures 3(a, b) display contours of constant values of instantaneous Reynolds stress (uv) and fluctuating vorticity magnitude ($|\boldsymbol{\omega}|^2$), respectively. Comparison with figure 2(b) suggests that slow pressure is concentrated in scales of roughly the same size as the Reynolds stress. In contrast, vorticity resides in scales considerably smaller in the transverse and more elongated in the direction of principal axes of the mean deformation-rate tensor. This is consistent with the observation of Rogers & Moin (1987) that vorticity concentrates in 'legs' of hairpin-like vortex structures as they are stretched and rotated by the mean shear.

4. Intercomponent energy transfer processes (events)

Statistical averages of the diagonal components of the rapid, slow and complete pressure–strain-rate tensor at $\beta = 4$ and 8 are presented in table 1. Statistically, the pressure–strain-rate transfers energy out of u ($T_{11} < 0$) into v and w ($T_{22} > 0$ and $T_{33} > 0$); the w-component receives the greater amount ($T_{33} > T_{22}$). The rapid term removes energy from u at a rate twice that of the slow term at $\beta = 4$ and at about the same rate at $\beta = 8$; however, the ratios between components of rapid transfer rate ($\Pi_{11}{:}\Pi_{22}{:}\Pi_{33}$) are nearly the same at both times.

† Only one-eighth of the whole $128 \times 128 \times 128$ dataset could be processed at a time on an IRIS workstation used for graphical display at the NASA-Ames Research Center. The strongest pressure–strain-rate events at $\beta = 8$ were observed in and near the plane shown.
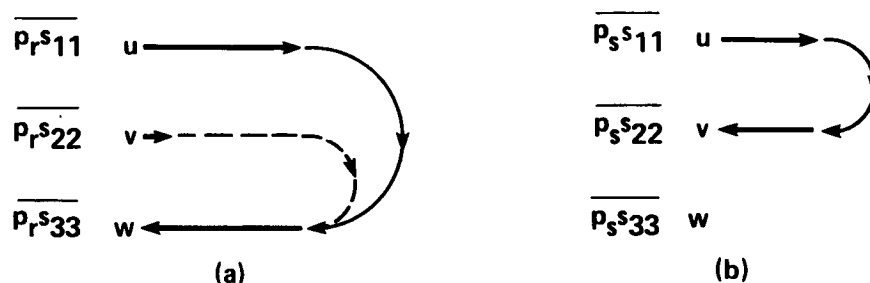
FIGURE 4. Schematic representation of intercomponent energy transfer process by pressure–strain-rate covariances ($\beta = 8$): (a) rapid transfer; (b) slow transfer. The directions of energy transfer are those suggested by the statistical averages.

The relative rate of gain or loss of energy in each component is illustrated schematically in figure 4. On average, both rapid and slow terms remove energy from u. Most of the net energy received by w is due to the rapid term, whereas the v-component receives its energy mostly via the slow term (see table 1). This would suggest, as indicated by the arrows, that the rapid term transfers energy from the u-component to the w-component (and a little from v to w), but the slow term delivers energy from the u-component directly to the v-component. The instantaneous field, however, shows that this is not the case.

Figures 5(a–c) show contours of constant slow pressure–strain-rate components at $\beta = 8$ on the xy-plane illustrated in figure 1. [N.B.: Negative values are contoured with solid lines and positive with dashed.] It can be observed that intercomponent energy transfer is highly localized in relatively few strong events.† Two-point correlations (not shown) suggest that the average spatial scale of the rapid transfer event is roughly twice that of the slow transfer event.

By comparing pressure–strain-rate contours in each of the three components, it is possible to determine the net sender and net receiver in each energy transfer event. Four events are identified for this purpose. Events Ⓐ and Ⓑ represent the greatest contributions to the energy transfer out of the u-component by the slow term.‡ Event Ⓐ is by far the strongest, reaching peak values twice that in Ⓑ. In this event, most of the energy from the u-component is transferred to the w-component and only a small amount of energy is transferred from u to v. Surrounding this event is a region of rather powerful energy transfer from the v-component into w-component. The w-component therefore receives energy both from u and v. A similar energy transfer process is seen in event Ⓑ, although most of the u-energy is transferred directly to w, with smaller amounts from u to v and v

---

† The rise in ps_{11} from zero is exceptionally abrupt. A three-dimensional view of constant ps_{11}-contours suggests that the transfer of energy from the u-component is concentrated in about ten primary events scattered within the $64 \times 64 \times 64$ subdomain.

‡ For the rapid transfer, two other exceptionally strong pressure–strain-rate events exist in addition to events coinciding with the two slow events.
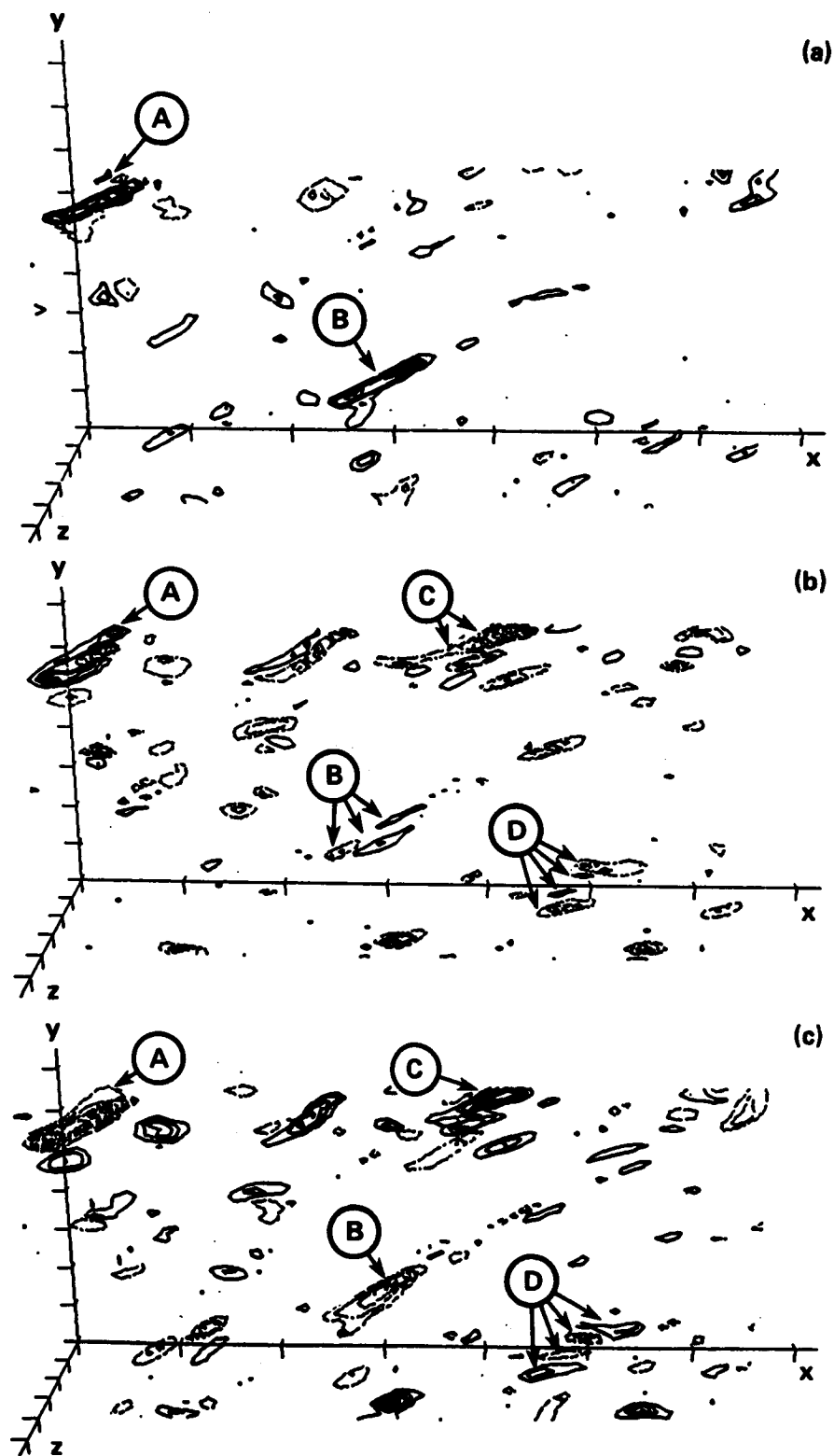
FIGURE 5. Contours of slow pressure–strain-rate on the xy-plane in figure 1 ($\beta = 8$): (a) $p_s s_{11}$; (b) $p_s s_{22}$; (c) $p_s s_{33}$. ——, negative; ----, positive. Four significant events are labeled (A), (B), (C) and (D) (see text).
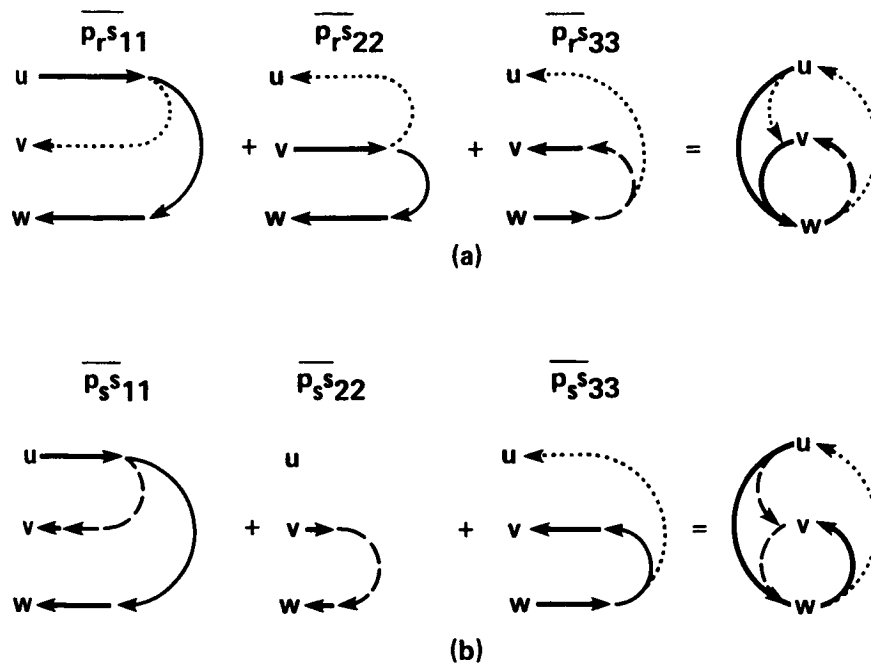
FIGURE 6. Schematic of the intercomponent energy transfer process as deduced from the instantaneous pressure–strain-rate field ($\beta = 8$): (a) rapid transfer; (b) slow transfer. A composite picture (on the right) is developed from sum of the individual energy transfer processes of the three components.

to w. Therefore, the slow term transfers most of the energy from u to w rather than to v (as might be implied by figure 4). In addition, a great deal of energy transfer takes place between v and w, independent of transfer from u. In event $\textcircled{C}$, for example, energy is transferred directly from the w-component to the v-component, and in event $\textcircled{D}$ energy flows back and forth between w and v.

Our interpretation of the instantaneous events in the rapid and slow pressure–strain-rate fields is schematically summarized in figure 6. The slow term transfers energy from u primarily to w with a small amount to v, and some energy from v is transferred to w; however, more energy enters v from w than vice versa. As shown to the right of figure 6, the net process is an indirect transfer of energy from u to v through w with significant energy transfer between v and w. The rapid term moves energy from u again primarily into w. However, there is considerably greater energy transfer to w from v. The w-component appears to receive a significant portion of its energy from the v-component, while transferring a lesser amount back to v. Compared with the slow process, the rapid term to a much greater extent transfers energy back to u from both v and w. The transfer processes in both rapid and slow parts are clearly more involved than those inferred from the statistics only (cf. fig. 4).
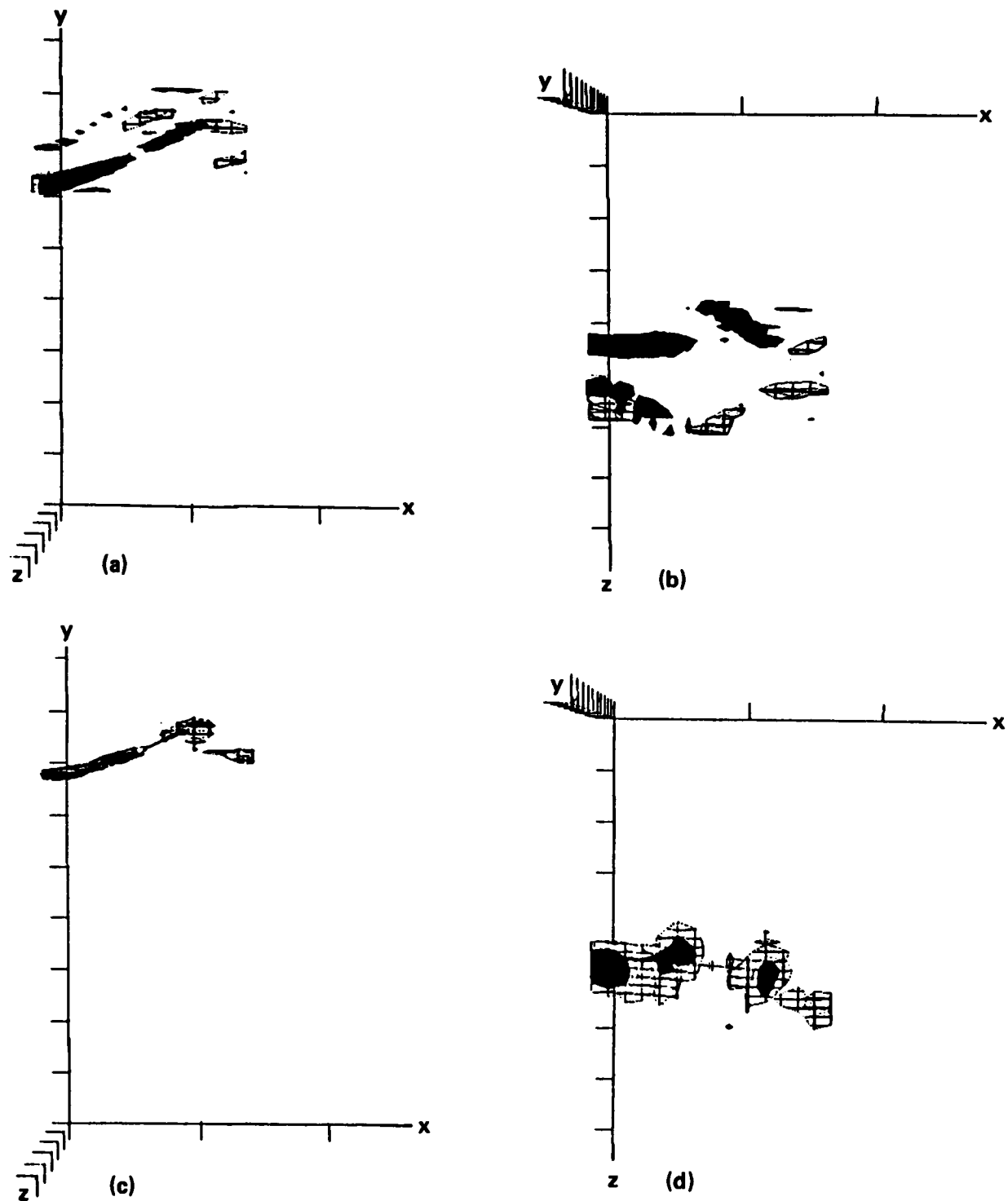
FIGURE 7. Three-dimensional contours of constant vorticity ($\beta = 8$): (a, b) ω_x, positive (solid contour) and negative (mesh contour); (c, d) ω_z, all negative (solid contour, higher values of $|\omega_z|$; mesh contour, lower values). (a, c) side view looking towards the xy-plane; (b, d) top view looking towards the xz-plane. (Very little positive ω_y exists in this region.)

5. Instantaneous structure of the most significant event

In their study of a sheared Taylor-Green cellular flow, Corrsin & Kollmann (1977) reported that intercomponent energy transfer from the streamwise to the transverse components is associated with local stagnation points. To understand the physical mechanisms by which the intercomponent energy transfer proceeds in homogeneous turbulent shear flow, the structure of the velocity field in the neighborhood of significant energy transfer events was investigated.

Event $\textcircled{A}$ in figure 5 shows the strongest energy transfer from the streamwise component in the $64 \times 64 \times 64$ subdomain at $\beta = 8$. Recall that this event is associated with a region of concentrated vorticity (fig. 3b). Upon close examination, we found a rather complex three-dimensional vortical structure in which the energy transfer event is embedded. In the xy-plane of figure 3(b), the fluctuating vorticity magnitide in event $\textcircled{A}$ turns out to be all spanwise vorticity ω_z (ω_x and ω_y are zero there!), indicative of the existence of a local shear layer. This is confirmed through three-dimensional contour plots of ω_x and ω_z near event $\textcircled{A}$ as shown in figure 7 (very little ω_y exists in this region).

The two vorticity components are viewed looking from the side along the z-axis at the xy-plane (figs. 7a, c) and looking from the top down at the xz-plane (figs. 7b, d). There exists a sheet of negative spanwise vorticity ($\omega_z < 0$) relatively thin in the y-direction in comparison with its spanwise extent (figs. 7c, d). Surrounding this sheet-like structure is a region of strong ω_x of two tube-like structures, one with positive and the other with negative streamwise vorticity (figs. 7a, b). The spanwise separation of the two vortex tubes was estimated to be about 20 viscous units ($\sqrt{\nu/S}$), consistent with the typical hairpin vortices observed by Rogers & Moin (1987) in the same flow. The vortical structure in the region of event $\textcircled{A}$ then appears to consist of the remnants of an inverted hairpin vortex with a local sheet of spanwise vorticity occupying the region in between.

Notice the gap in the spanwise vorticity shown in figure 7(d). Examination of the velocity vectors shows the existence of a local stagnation point in this gap, apparently a consequence of the velocity field induced locally by the vortical structure. Figure 8(a) shows the top view of the three-dimensional region in which ps_{11} is concentrated compared with streamwise (fig. 7b) and spanwise vorticity (fig. 7d). The peak in ps_{11} (solid volume) occupies this gap in the ω_z-field, suggesting the energy transfer out of the u-component is, for this powerful event, associated with a local stagnation point, itself associated with neighboring vortical structures embedded in the turbulent field. Interestingly, instantaneous Reynolds stress (fig. 8b), like streamwise vorticity, is concentrated in regions which straddle the ps_{11}-event.

As we have observed, the structure of high pressure–strain-rate concentration interacts strongly with coherent vortical structure where the Reynolds-stress eddies are energetic. In view of its importance of the pressure–strain-rate term in Reynolds-stress transport modeling, it would be of considerable value to investigate how the intercomponent energy transfer by the pressure–strain-rate takes place in association with dynamics of the coherent vortical structures.
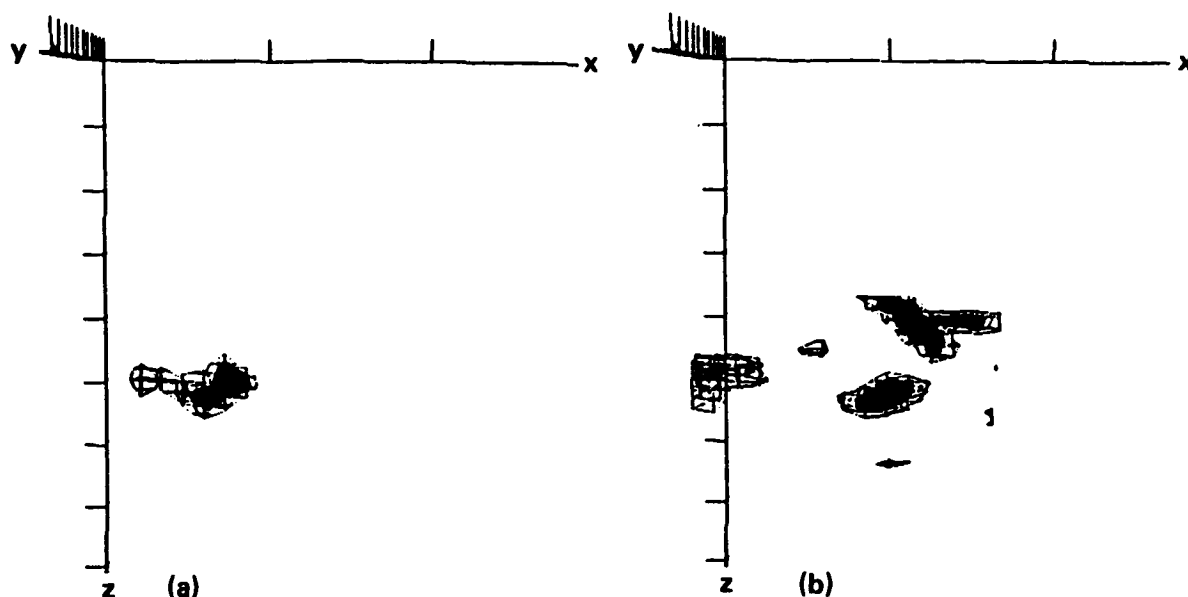
FIGURE 8. Three-dimensional contours in top view looking towards the xz-plane ($\beta = 8$): (a) pressure–strain-rate, ps_{11}; (b) Reynolds stress, uv. In both plots, contours shown are all negative (solid contour, higher values in negative; mesh contour, lower values).

REFERENCES

BATCHELOR, G. K. 1953 *The theory of homogeneous turbulence*. Cambridge University Press: Cambridge, England.

CORRSIN, S. & KOLLMANN, W. 1977 Preliminary report on sheared cellular motion as a qualitative model of homogeneous turbulent shear flow. In *Turbulence in Internal Flows*, a 1976 Project SQUID Workshop (ed. S. N. B. Murthy), pp. 11–33. Hemisphere Publ. Corp.: Washington, D.C.

HARRIS, V. G., GRAHAM, J. A. H. & CORRSIN, S. 1977 Further experiments in nearly homogeneous turbulent shear flow. *J. Fluid Mech.* **81**, 657–687.

KIM, J., MOIN, P. & MOSER, R. D. 1987 Turbulence statistics in fully developed channel flow at low Reynolds number. *J. Fluid Mech.* **177**, 133–166.

LAUNDER, B. E., REECE, G. J. & RODI, W. 1975 Progress in the development of a Reynolds-stress turbulence closure. *J. Fluid Mech.* **68**, 537–566.

LEE, M. J., KIM, J. & MOIN, P. 1987 Turbulence structure at high shear rate. In *Proc. Sixth Symp. on Turbent Shear Flows*, Toulouse, France, Sept. 7–9, 1987 (ed. F. Durst *et al.*), pp. 22.6.1–22.6.6.

LEE, M. J. & REYNOLDS, W. C. 1987 Structure and modeling of homogeneous turbulence in strain and relaxation processes. (Submitted to *J. Fluid Mech.*)

LUMLEY, J. L. 1975 Pressure-strain correlation. *Phys. Fluids* **18**, 750.

LUMLEY, J. L. 1978 Computational modeling of turbulent flows. *Adv. Appl. Mech.* **18**, 123–176.

ROGALLO, R. S. 1981 Numerical experiments in homogeneous turbulence. *NASA Tech. Memo.* 81315.

ROGERS, M. M. & MOIN, P. 1987 The structure of the vorticity field in homogeneous turbulent flows. *J. Fluid Mech.* **176**, 33–66.

ROGERS, M. M., MOIN, P. & REYNOLDS, W. C. 1986 The structure and modeling of the hydrodynamic and passive scaler fields in homogeneous turbulent shear flow. *Dept. Mech. Engng. Rep.* TF–25, Stanford University: Stanford, California.

TAVOULARIS, S. & CORRSIN, S. 1981 Experiments in nearly homogeneous turbulent shear flow with a uniform mean temperature gradient. *J. Fluid Mech.* **104**, 311–347.